

Electromagnetic fields with electric and chiral magnetic conductivities in heavy ion collisions

Hui Li, Xin-li Sheng, and Qun Wang

*Interdisciplinary Center for Theoretical Study and Department of Modern Physics,
University of Science and Technology of China, Hefei, Anhui 230026, China*

We derive analytic formula for electric and magnetic fields produced by a moving charged particle in a conducting medium with the electric conductivity σ and the chiral magnetic conductivity σ_χ . We use the Green function method and assume that σ_χ is much smaller than σ . The compact algebraic expressions for electric and magnetic fields without any integrals are obtained. They recover the Lienard-Wiechert formula at vanishing conductivities. Exact numerical solutions are also found for any values of σ and σ_χ and are compared to analytic results. Both numerical and analytic results agree very well for the scale of high energy heavy ion collisions. The space-time profiles of electromagnetic fields in non-central Au+Au collisions have been calculated based on these analytic formula as well as exact numerical solutions.

I. INTRODUCTION

Strong electromagnetic fields are generated in peripheral heavy-ion collisions (HIC), which provides a good opportunity for studying rich phenomena related to strong fields. At the collisional energy \sqrt{s} per nucleon which is much larger than the nucleon mass m_n , the nucleons are moving with the velocity $v = \sqrt{(s - m_n^2)/s} \sim 1 - m_n^2/(2s)$ which is almost speed of light with a large Lorentz contraction factor $\gamma = 1/\sqrt{1 - v^2/c^2} \sim \sqrt{s}/m_n$. The typical electric field in the co-moving frame of one nucleus can be estimated by the Coulomb law, Ze/R_A^2 , with Z and R_A being the proton number and the radius of the nucleus respectively. The magnetic field in the lab frame can be approximated as the product of the Lorentz factor and the electric field in the co-moving frame of the nucleus, $eB \sim \gamma v Ze^2/R_A^2$. In Au+Au collisions at the Relativistic Heavy Ion Collider (RHIC) at $\sqrt{s} = 200$ GeV, the peak value of the magnetic field at the moment of the collision is about $5m_\pi^2$ (m_π : pion mass) or 1.4×10^{18} Gauss. In Pb+Pb collisions at the Large Hadron Collider (LHC) at $\sqrt{s} = 2.76$ TeV, the peak value of the magnetic field can be 10 times as large as at RHIC.

Since the magnitude of the electromagnetic fields enter the regime of strong interaction, the effects of such enormous fields are expected to be observable in the final hadronic events in HIC. In recent years there have been many efforts to investigate such effects, among which the interplay between strong magnetic fields and quantum anomaly leads to a group of related phenomena, such as the Chiral Magnetic Effect (CME) [1, 2], the Chiral Vortical Effect [3, 4], and the Chiral Magnetic Wave [5], the Chiral Vortical Wave [6], etc.. For reviews of recent developments, see, e.g. [7, 8]. All these effects are related to chiral properties of fermions, especially massless fermions or chiral fermions. The movement of chiral fermions can be described by the chiral kinetic equations which incorporate structures of Berry phase and monopole in momentum space [9–18]. The charge separation effect observed in the STAR and ALICE experiments can be well described by the CME [19–21], but no definite conclusion has been made that the charge separation effect results unambiguously and exclusively from the CME instead of the collective expansion of the fireball.

As a starting point to study these phenomena, one must know the space-time profile of electromagnetic fields in HIC. Several earlier calculations [1, 22–24] as well as later calculations including event-by-event fluctuations [25, 26] show that the electromagnetic fields peak almost at the time of collision and disappear in very short time after the collision. For example, the magnetic field along the global angular momentum falls rapidly by $\sim 1/t^3$. At $\sqrt{s} = 200$ GeV, it drops by two to three orders of magnitude in about 0.5 fm/c from the collision time. If this is the case, one cannot expect a sizable influence on the final state hadrons in late time from such short pulses of magnetic fields. However the medium effects have not been considered in these calculations. The main response of the plasma to the fields is the electric conduction. The electric conductivity is proportional to plasma temperature, which is a function of time because the plasma is expanding. In strong coupling regime, electric conductivity can be calculated by lattice gauge theory [27, 28] and holographic models [29]. Ohm's currents will be induced in the plasma and slow down the decrease of the fields [30, 31]. To study the CME effect, one has to include the CME conductivity σ_χ . The electromagnetic fields produced by a point charge with σ_χ and σ have been calculated analytically in Ref. [32] but only for the relativistic limit ($v = 1$). The numerical and analytic calculations with σ but without σ_χ were done in Ref. [30, 31]. The directed flow of charged hadrons in HIC has been studied with non-vanishing σ but without σ_χ in Ref. [33] by calculating the velocity shift of each fluid cell due to electromagnetic

force in the hydrodynamic evolution.

In this paper, we will solve the Maxwell equations both analytically and numerically for a moving point charge in a conducting medium with non-vanishing σ and σ_χ . We use the method of the Green functions under the condition $\sigma_\chi \ll \sigma$ which is valid for high energy HIC. Analytic expressions of electric and magnetic fields are given for finite σ and small values of σ_χ without taking the relativistic limit ($v = 1$). The numerical results for finite σ and σ_χ agree perfectly with the analytic results. Finally we carry out the numerical calculations for the electromagnetic fields in non-central Au+Au collisions at $\sqrt{s} = 200$ GeV. Normally one uses the AMPT model [34], the HIJING model [35], or the UrQMD model [36] to simulate the collision processes and to calculate the electromagnetic fields. In this paper, we will use the UrQMD model to give the space-time and momentum configuration of charged particles in HIC the calculations with vanishing σ and σ_χ , but we will use a kinematic model for participant nucleons with non-vanishing σ and σ_χ . Generally the strong magnetic fields will influence the evolution of the particle system [37], which we will not consider in our calculations.

The paper is organized as follows. In Section II, we give the formal solution to the Maxwell equations with σ and σ_χ using the method of Green functions. In Section III and IV, we derive analytic expressions for magnetic and electric fields of a point charge respectively. We give in Section V numerical results for electromagnetic fields produced in non-central Au+Au collisions at $\sqrt{s} = 200$ GeV. A summary of results is given in Section VI.

We will adopt following conventions for three-dimensional (3D) or two-dimensional (2D) vectors. We will use Roman letters in boldface for 3D or 2D vectors. In Cartesian coordinates, three orthogonal components of a 3D vector are denoted as plain Roman letters with subscripts x, y, z . A point in coordinate space is written as $\mathbf{x} = (x, y, z) = (\mathbf{x}_T, z)$, where \mathbf{x}_T represents its 2D component. Similarly a momentum is written as $\mathbf{k} = (k_x, k_y, k_z) = (\mathbf{k}_T, k_z)$. The vectors of the electric and magnetic fields are written as $\mathbf{E} = (E_x, E_y, E_z)$ and $\mathbf{B} = (B_x, B_y, B_z)$. We will also use cylindrical coordinate whose longitudinal component is chosen to be the third component of Cartesian coordinate, e.g., $\mathbf{x} = (x_T, \phi, z)$ with $x_T = |\mathbf{x}_T|$.

II. FIELD EQUATIONS AND THEIR FORMAL SOLUTIONS

We consider an infinite homogeneous medium whose conducting property can be described by a constant electric conductivity σ and a constant chiral magnetic conductivity σ_χ . These requirements give us the most simplified model for conducting medium with the chiral magnetic effect (CME). In this medium, the total currents can be decomposed into three parts, the external current, the Ohm's current ($\sigma\mathbf{E}$) induced by the electric field \mathbf{E} , and the chiral magnetic current ($\sigma_\chi\mathbf{B}$) induced by the magnetic field \mathbf{B} . The Maxwell equations read

$$\begin{aligned}\nabla \cdot \mathbf{E} &= \frac{\rho_{\text{ext}}}{\epsilon}, \\ \nabla \cdot \mathbf{B} &= 0, \\ \nabla \times \mathbf{E} &= -\partial_t \mathbf{B}, \\ \nabla \times \mathbf{B} &= \partial_t \mathbf{E} + \mathbf{J}_{\text{ext}} + \sigma \mathbf{E} + \sigma_\chi \mathbf{B},\end{aligned}\tag{1}$$

where ρ_{ext} and \mathbf{J}_{ext} denote the external charge and current densities respectively. One should note that in general the permittivity, $\epsilon(\omega) = 1 + i\sigma/\omega$, depends on the frequency. Taking curl of the third and the fourth line in Eq. (1) and using the first and the second line, we obtain,

$$\begin{aligned}(\nabla^2 - \partial_t^2 - \sigma\partial_t) \mathbf{B} + \sigma_\chi \nabla \times \mathbf{B} &= -\nabla \times \mathbf{J}_{\text{ext}}, \\ (\nabla^2 - \partial_t^2 - \sigma\partial_t) \mathbf{E} + \sigma_\chi \nabla \times \mathbf{E} &= \frac{1}{\epsilon} \nabla \rho_{\text{ext}} + \partial_t \mathbf{J}_{\text{ext}}.\end{aligned}\tag{2}$$

It is obvious that both the magnetic and electric fields satisfy the same system of partial differential equations,

$$\hat{L}\mathbf{F}(t, \mathbf{x}) + \sigma_\chi \nabla \times \mathbf{F}(t, \mathbf{x}) = \mathbf{f}(t, \mathbf{x}).\tag{3}$$

Here $\mathbf{F}(t, \mathbf{x})$ is a vector representing \mathbf{B} or \mathbf{E} . The partial differential operator is defined as $\hat{L} = \nabla^2 - \partial_t^2 - \sigma\partial_t$. The function $\mathbf{f}(t, \mathbf{x})$ on the right-hand-side stands for the source terms in Eq. (2). We can also write Eq. (3) in a matrix form in terms of three components of $\mathbf{F} = (F_x, F_y, F_z)$ and

$$\mathbf{f} = (f_x, f_y, f_z),$$

$$\begin{pmatrix} \hat{L} & -\sigma_\chi \partial_z & \sigma_\chi \partial_y \\ \sigma_\chi \partial_z & \hat{L} & -\sigma_\chi \partial_x \\ -\sigma_\chi \partial_y & \sigma_\chi \partial_x & \hat{L} \end{pmatrix} \begin{pmatrix} F_x \\ F_y \\ F_z \end{pmatrix} (t, \mathbf{x}) = \begin{pmatrix} f_x \\ f_y \\ f_z \end{pmatrix} (t, \mathbf{x}). \quad (4)$$

where we have used the shorthand notation $\nabla = (\partial/\partial x, \partial/\partial y, \partial/\partial z) \equiv (\partial_x, \partial_y, \partial_z)$.

Now we are at the point to solve the above equation. To this end, it is convenient to work in momentum space and expand $\mathbf{F}(t, \mathbf{x})$ and $\mathbf{f}(t, \mathbf{x})$ as

$$\begin{aligned} \mathbf{F}(t, \mathbf{x}) &= \int \frac{d\omega d^3\mathbf{k}}{(2\pi)^4} e^{-i\omega t + i\mathbf{k}\cdot\mathbf{x}} \mathbf{F}(\omega, \mathbf{k}), \\ \mathbf{f}(t, \mathbf{x}) &= \int \frac{d\omega d^3\mathbf{k}}{(2\pi)^4} e^{-i\omega t + i\mathbf{k}\cdot\mathbf{x}} \mathbf{f}(\omega, \mathbf{k}). \end{aligned} \quad (5)$$

Insert the above expressions into Eq. (4), we obtain by making replacement $\partial_t \rightarrow -i\omega$, $\nabla \rightarrow i\mathbf{k}$,

$$\begin{pmatrix} L & -i\sigma_\chi k_z & i\sigma_\chi k_y \\ i\sigma_\chi k_z & L & -i\sigma_\chi k_x \\ -i\sigma_\chi k_y & i\sigma_\chi k_x & L \end{pmatrix} \begin{pmatrix} F_x \\ F_y \\ F_z \end{pmatrix} (\omega, \mathbf{k}) = \begin{pmatrix} f_x \\ f_y \\ f_z \end{pmatrix} (\omega, \mathbf{k}), \quad (6)$$

where $L = \omega^2 + i\sigma\omega - k^2$ and $k = |\mathbf{k}|$. We can write the coefficient matrix in a compact form,

$$M_{ij} = L\delta_{ij} - i\sigma_\chi \epsilon_{ijl} k_l, \quad (7)$$

with the determinant

$$\det M = L(L^2 - \sigma_\chi^2 k^2). \quad (8)$$

In Eq. (7) we have used the notation $\mathbf{k} = (k_x, k_y, k_z) = (k_1, k_2, k_3)$. If $\det M \neq 0$, we can get the inverse of M given by its adjoint matrix divided by its determinant,

$$M^{-1} = \frac{1}{\det M} \begin{pmatrix} L^2 - \sigma_\chi^2 k_x^2 & iL\sigma_\chi k_z - \sigma_\chi^2 k_x k_y & -iL\sigma_\chi k_y - \sigma_\chi^2 k_x k_z \\ -iL\sigma_\chi k_z - \sigma_\chi^2 k_x k_y & L^2 - \sigma_\chi^2 k_y^2 & iL\sigma_\chi k_x - \sigma_\chi^2 k_y k_z \\ iL\sigma_\chi k_y - \sigma_\chi^2 k_x k_z & -iL\sigma_\chi k_x - \sigma_\chi^2 k_y k_z & L^2 - \sigma_\chi^2 k_z^2 \end{pmatrix}. \quad (9)$$

With M^{-1} we can write down the solution to Eq. (6) as

$$\mathbf{F}(\omega, \mathbf{k}) = \frac{1}{L^2 - \sigma_\chi^2 k^2} [L\mathbf{f}(\omega, \mathbf{k}) - i\sigma_\chi \mathbf{k} \times \mathbf{f}(\omega, \mathbf{k})] - \frac{\sigma_\chi^2}{L(L^2 - \sigma_\chi^2 k^2)} \mathbf{k}[\mathbf{k} \cdot \mathbf{f}(\omega, \mathbf{k})], \quad (10)$$

where the source terms $\mathbf{f}(\omega, \mathbf{k})$ are given by

$$\mathbf{f}(\omega, \mathbf{k}) = \begin{cases} -i\mathbf{k} \times \mathbf{J}_{\text{ext}}(\omega, \mathbf{k}), & \text{for } \mathbf{B} \\ i\mathbf{k} \frac{\rho_{\text{ext}}(\omega, \mathbf{k})}{1+i\sigma/\omega} - i\omega \mathbf{J}_{\text{ext}}(\omega, \mathbf{k}), & \text{for } \mathbf{E} \end{cases} \quad (11)$$

We note that the second term $\sim \sigma_\chi^2 \mathbf{k}[\mathbf{k} \cdot \mathbf{f}(\omega, \mathbf{k})]$ in Eq. (10) is obviously vanishing for \mathbf{B} , but it is not vanishing for \mathbf{E} . Using the charge conservation equation $\partial\rho_{\text{ext}}/\partial t + \nabla \cdot \mathbf{J}_{\text{ext}} = 0$, this term for \mathbf{E} is proportional to $\sim [(L^2 - \sigma_\chi^2 k^2)(1 + i\sigma/\omega)]^{-1}$. From the poles of $\mathbf{F}(\omega, \mathbf{k})$, we can obtain the dispersion relations $\omega(\mathbf{k})$ for collective modes of electromagnetic fields. The poles of the first term (or of \mathbf{B}) in Eq. (10) are given by the roots of $L^2 - \sigma_\chi^2 k^2 = 0$, which are $\omega_{s_1 s_2} = -i\sigma/2 + s_1 \sqrt{k^2 + s_2 k \sigma_\chi - \sigma^2/4}$ ($s_1, s_2 = \pm 1$). For \mathbf{E} , the second term in Eq. (10) introduces an additional pole $\omega = -i\sigma$ besides $\omega_{s_1 s_2}$. These poles give the collective modes of the fields without external sources, where ω and \mathbf{k} are independent variables. For external charges with ρ_{ext} and \mathbf{J}_{ext} , the dispersion relations will be modified due to additional relations between ω and \mathbf{k} , e.g., in the next section we will consider a point charge moving along the z -direction which introduces the constraint $\omega = vk_z$.

III. MAGNETIC FIELDS OF A MOVING CHARGE

A. Integration over the polar angle and longitudinal momentum

In this section, we will derive an analytical expression for the magnetic field of a charged particle. Without loss of generality, we consider the situation that the charged particle (with charge Q) moves along the third axis direction. More general cases along arbitrary directions can be obtained by rotation. In heavy ion collisions, generally the CME conductivity is a small quantity compared to the electric one. The charge density and the current density read,

$$\begin{aligned}\rho(t, \mathbf{x}) &= Q\delta(x)\delta(y)\delta(z-vt), \\ \mathbf{J}(t, \mathbf{x}) &= Qv\delta(x)\delta(y)\delta(z-vt)\mathbf{e}_z.\end{aligned}\quad (12)$$

In momentum space, they are in the form

$$\begin{aligned}\rho(\omega, \mathbf{k}) &= 2\pi Q\delta(\omega - k_z v), \\ \mathbf{J}(\omega, \mathbf{k}) &= 2\pi Qv\delta(\omega - k_z v)\mathbf{e}_z.\end{aligned}\quad (13)$$

Here we denote three directions in flat coordinate space as $(\mathbf{e}_x, \mathbf{e}_y, \mathbf{e}_z)$. In cylindrical coordinates, we denote three orthogonal directions as $(\mathbf{e}_r, \mathbf{e}_\phi, \mathbf{e}_z)$. Inserting Eq. (13) into Eqs. (10,11), we obtain the magnetic field in momentum space,

$$\begin{pmatrix} B_x \\ B_y \\ B_z \end{pmatrix}(\omega, \mathbf{k}) = -2\pi i Q v \frac{\delta(\omega - k_z v)}{L^2 - \sigma_\chi^2 k^2} \begin{pmatrix} Lk_y - i\sigma_\chi k_x k_z \\ -Lk_x - i\sigma_\chi k_y k_z \\ i\sigma_\chi(k_x^2 + k_y^2) \end{pmatrix}.\quad (14)$$

We can transform Eq. (14) back to coordinate space. This involves integration over ω and \mathbf{k} . Since the charged particle moves along the third direction, it is convenient to work in the cylindrical coordinate (r, ϕ, z) . So we can write $\mathbf{k} \cdot \mathbf{x} = \mathbf{k}_T \cdot \mathbf{x}_T + k_z z = k_T x_T \cos\theta + k_z z$, where we have assumed that the angle between \mathbf{x}_T and \mathbf{k}_T is θ . We can easily integrate over k_z from Eq. (14), which removes the delta function with k_z being set to ω/v in the integrand,

$$\begin{aligned}\begin{pmatrix} B_r \\ B_\phi \\ B_z \end{pmatrix}(t, \mathbf{x}) &= -iQ \int \frac{d\omega d\theta dk_T}{(2\pi)^3} e^{-i\omega(t-z/v) + ik_T x_T \cos\theta} \frac{k_T^2}{D(\omega, k_T)} \\ &\times \left[L(\omega, k_T) \begin{pmatrix} \sin\theta \\ -\cos\theta \\ 0 \end{pmatrix} + \frac{i\sigma_\chi}{v} \begin{pmatrix} -\omega \cos\theta \\ -\omega \sin\theta \\ vk_T \end{pmatrix} \right],\end{aligned}\quad (15)$$

where we have chosen that \mathbf{x}_T is along \mathbf{e}_x , so \mathbf{e}_r (\mathbf{e}_x) is in the direction of \mathbf{x}_T and \mathbf{e}_ϕ (\mathbf{e}_y) is in the direction of $\mathbf{e}_z \times \mathbf{e}_r$. We have used in Eq. (15)

$$\begin{aligned}L(\omega, k_T) &= -\frac{1}{v^2 \gamma^2} \omega^2 + i\sigma\omega - k_T^2, \\ D(\omega, k_T) &= L^2(\omega, k_T) - \sigma_\chi^2 \frac{\omega^2}{v^2} - \sigma_\chi^2 k_T^2.\end{aligned}\quad (16)$$

Integration over θ can be done using cylindrical Bessel functions, $\int_0^{2\pi} d\theta e^{ik_T x_T \cos\theta} = 2\pi J_0(k_T x_T)$ and $\int_0^{2\pi} d\theta e^{ik_T x_T \cos\theta} \cos\theta = 2\pi i J_1(k_T x_T)$. Inserting these into Eq. (15), we can have a simple form,

$$\mathbf{B}(t, \mathbf{x}) = -Q \int \frac{d\omega dk_T}{(2\pi)^2} \frac{\mathbf{B}'(\omega, k_T)}{D(\omega, k_T)},\quad (17)$$

where $\mathbf{B}'(\omega, k_T)$ can be defined in cylindrical coordinates as follows

$$\begin{aligned}\begin{pmatrix} B'_r \\ B'_\phi \\ B'_z \end{pmatrix}(\omega, k_T) &\equiv k_T^2 e^{-i\omega(t-z/v)} \\ &\times \left[L(\omega, k_T) \begin{pmatrix} 0 \\ J_1(k_T x_T) \\ 0 \end{pmatrix} + \frac{\sigma_\chi}{v} \begin{pmatrix} i\omega J_1(k_T x_T) \\ 0 \\ -vk_T J_0(k_T x_T) \end{pmatrix} \right],\end{aligned}\quad (18)$$

where J_0 and J_1 are Bessel functions of the first kind. Note that the integral over ω in Eq. (17) is from $-\infty$ to $+\infty$. We can easily prove that the right-hand side of Eq. (17) is a real number. We see in the integrand that ω is always accompanied by an imaginary unit i . If we replace ω with $-\omega$ in the integrand, we will get exactly its complex conjugate, so the the integral over ω in Eq. (17) can be replaced by an integral of the real part over ω from 0 to $+\infty$.

B. Integration over frequency

To carry out the integration over ω , we need to make analytic continuation for the frequency to complex plane and calculate the residues of singularities. The denominator $D(\omega, k_T)$ in Eq. (17) is a quartic polynomial of ω . For a fixed k_T , $D(\omega, k_T)$ has four roots in the complex plane, each of which gives a pole of the integrand. In high energy heavy ion collisions, the Ohm conductivity σ is much larger than the chiral magnetic conductivity σ_χ , so it is reasonable to treat σ_χ as a perturbation.

Now we deal with the poles of the integrand in Eq. (17). To this end, we need to find the roots of the equation $D(\omega, k_T) = 0$. For a fixed value of k_T , we assume the solutions take the following form

$$\omega = \omega_0 + \sigma_\chi c_1 + \sigma_\chi^2 c_2 + \dots, \quad (19)$$

where the zero-th order value ω_0 denote the roots of the equation $L(\omega, k_T) = 0$ and are given by

$$\omega_\pm \equiv iv\gamma \frac{1}{2} \left[v\gamma\sigma \pm \sqrt{(v\gamma\sigma)^2 + 4k_T^2} \right]. \quad (20)$$

We see that the zero-th order solutions are doublet. We insert Eq. (19) into $D(\omega, k_T)$ and expand in powers of σ_χ . When implementing $\omega_0 = \omega_\pm$ in $D(\omega, k_T)$, the zero-th and first order terms in σ_χ are vanishing. The coefficient c_1 appears in the σ_χ^2 term and can be determined by the condition that it vanishes. Implementing the values of c_1 , we can determine c_2 from the vanishing of σ_χ^3 term. Putting them together, we obtain the roots in the following form

$$\omega_{s_1 s_2} \equiv \omega_{s_1} + s_2 \sigma_\chi c_{s_1}^{(1)} + \sigma_\chi^2 c_{s_1}^{(2)}, \quad (s_1, s_2 = \pm 1), \quad (21)$$

where $c_{s_1}^{(1)}$ and $c_{s_1}^{(2)}$ are given by

$$\begin{aligned} c_s^{(1)} &= \frac{v\gamma^2 \sqrt{(v\gamma\sigma)^2 + 2v^2 k_T^2} + s(v\gamma\sigma) \sqrt{(v\gamma\sigma)^2 + 4k_T^2}}{\sqrt{2} \sqrt{(v\gamma\sigma)^2 + 4k_T^2}}, \\ c_s^{(2)} &= -s \frac{iv\gamma^3 k_T^2 (2 - v^2)}{[(v\gamma\sigma)^2 + 4k_T^2]^{3/2}}. \end{aligned} \quad (22)$$

The polynomial $D(\omega, k_T)$ can thus be expressed in terms of these four roots in (21),

$$D(\omega, k_T) = \frac{1}{(v\gamma)^4} \prod_{s_1, s_2 = \pm} (\omega - \omega_{s_1 s_2}). \quad (23)$$

It is easy to verify that ω_{++} and ω_{+-} are located in the upper half complex plane and ω_{--} are located in the lower half one, while ω_{-+} is located in the lower half plane when $\sigma_\chi < k_T$. For a relativistic particle in heavy ion collisions, the condition $\sigma_\chi < k_T$ is satisfied in most cases [32]. So we treat ω_{-+} as a pole located in the lower half plane.

To the linear order in σ_χ , the differences between two poles in the upper and lower half plane are

$$\begin{aligned} \Delta\omega_+ &= \omega_{++} - \omega_{+-} \approx 2\sigma_\chi c_+^{(1)} \rightarrow 2\sigma_\chi v\gamma^2, \quad \text{for } k_T = 0 \\ \Delta\omega_- &= \omega_{-+} - \omega_{--} \approx 2\sigma_\chi c_-^{(1)} \rightarrow 0, \quad \text{for } k_T = 0 \end{aligned} \quad (24)$$

We see that $\Delta\omega_+$ ($\Delta\omega_-$) is non-vanishing (vanishing) at $k_T = 0$. For the imaginary part in Eq. (20), we see $|\omega_+| \geq (v\gamma)^2 \sigma$, i.e. it has non-zero lower bound but $|\omega_-| \geq 0$ has zero bound, where the equality holds at $k_T = 0$ for both cases. The poles in upper (lower) half plane whose imaginary part is ω_+ (ω_-) give the advanced (retarded) solution with $vt - z < 0$ ($vt - z > 0$). Such a difference in the imaginary part makes the advanced solution more suppressed than the retarded one at relativistic limit with $\gamma \gg 1$.

Then we can carry out the integration over ω by contour integration. For the advanced (retarded) region $vt < z$ ($vt > z$), we need to close the contour in the upper (lower) half plane and pick up two poles $\omega_{+, \pm}$ ($\omega_{-, \pm}$). The residues of $D^{-1}(\omega, k_T)$ at poles are given by

$$R_{s_1 s_2}(k_T) \equiv \lim_{\omega \rightarrow \omega_{s_1 s_2}} \frac{\omega - \omega_{s_1 s_2}}{D(\omega, k_T)} \approx \frac{(v\gamma)^4}{2\sigma_\chi c_{s_1}^{(1)} (\delta\omega)^2} \left(s_2 - s_1 \frac{2\sigma_\chi c_{s_1}^{(1)}}{\delta\omega} \right), \quad (25)$$

where $\delta\omega \equiv \omega_+ - \omega_- = iv\gamma\sqrt{(v\gamma\sigma)^2 + 4k_T^2}$ is the difference between two roots in Eq. (20). Thus the integration over ω can be done by applying the residue theorem,

$$\begin{aligned} \mathbf{B}(t, \mathbf{x}) &= -i\theta\left(\frac{z}{v} - t\right)Q \int \frac{dk_T}{2\pi} \sum_{s=\pm} \mathbf{B}'(\omega_{+,s}, k_T) R_{+,s}(k_T) \\ &\quad + i\theta\left(t - \frac{z}{v}\right)Q \int \frac{dk_T}{2\pi} \sum_{s=\pm} \mathbf{B}'(\omega_{-,s}, k_T) R_{-,s}(k_T), \end{aligned} \quad (26)$$

where the terms of $\theta(\frac{z}{v} - t)$ and $\theta(t - \frac{z}{v})$ correspond to advanced and retarded contributions respectively.

C. Algebraic expressions for magnetic fields

After carrying out the k_T integral, we obtain an algebraic expression for the tangential component B_ϕ in the leading order in σ_χ ,

$$B_\phi(t, \mathbf{x}) = \frac{Q}{4\pi} \cdot \frac{v\gamma x_T}{\Delta^{3/2}} \left(1 + \frac{\sigma v\gamma}{2} \sqrt{\Delta} \right) e^A. \quad (27)$$

Here we have defined symbols $\Delta \equiv \gamma^2(vt - z)^2 + x_T^2$ and $A \equiv (\sigma v\gamma/2)[\gamma(vt - z) - \sqrt{\Delta}]$ (note that $A < 0$). It is easy to verify that B_ϕ in Eq. (27) recovers the formula from Lienard-Wiechert potentials when $\sigma = 0$. We note that such a form of B_ϕ was first given in Ref. [33]. The linear order contribution in σ_χ is absent in B_ϕ . This means that the chiral magnetic effect characterized by σ_χ does not play a major role in the tangential component. However the major correction is from electric conductivity.

For the radial and longitudinal components, we now give following simple algebraic expressions in the leading order in σ_χ ,

$$\begin{aligned} B_r(t, \mathbf{x}) &= -\sigma_\chi \frac{Q}{8\pi} \cdot \frac{v\gamma^2 x_T}{\Delta^{3/2}} \left[\gamma(vt - z) + A\sqrt{\Delta} \right] e^A, \\ B_z(t, \mathbf{x}) &= \sigma_\chi \frac{Q}{8\pi} \cdot \frac{v\gamma}{\Delta^{3/2}} \left[\gamma^2(vt - z)^2 \left(1 + \frac{\sigma v\gamma}{2} \sqrt{\Delta} \right) + \Delta \left(1 - \frac{\sigma v\gamma}{2} \sqrt{\Delta} \right) \right] e^A. \end{aligned} \quad (28)$$

We see that they are proportional to σ_χ . Previous studies have shown that the electric conducting effect will never generate B_r and B_z , so these non-vanishing components are the result of the chiral magnetic effect. This can be easily understood: a moving charge produces magnetic fields in the tangential direction, which then turns into a tangential current due to the chiral magnetic effect and finally generates B_r and B_z .

We now make a few comments about advanced and retarded contributions in Eqs. (27,28). We see that $\theta(\frac{z}{v} - t)$ and $\theta(t - \frac{z}{v})$ which characterize the advanced and retarded contributions disappear, the reason is that the rest expressions apart from the theta-functions are identical in both contributions, therefore we can combine them as $\theta(\frac{z}{v} - t) + \theta(t - \frac{z}{v}) = 1$. The presence of the factor e^A shows that the advanced contribution is suppressed exponentially relative to the retarded one, since the $\sigma\gamma^2(vt - z)$ part in A is negative (positive) for the advanced (retarded) parts.

One can verify that the higher order corrections to B_ϕ , B_r and B_z are all of $O(\sigma_\chi^2)$. At very late time, one can see from Eqs. (27,28) that the fields decay in time as $B_{\phi,r} \sim 1/t^2$ and $B_z \sim 1/t$.

D. Relativistic limit

In this subsection, we consider the relativistic limit with $v \sim 1$ and $\gamma \gg 1$. Eq. (16) becomes,

$$\begin{aligned} L(\omega, k_T) &\approx i\sigma\omega - k_T^2, \\ D(\omega, k_T) &\approx (i\sigma\omega - k_T^2)^2 - \sigma_\chi^2\omega^2 - \sigma_\chi^2 k_T^2. \end{aligned} \quad (29)$$

The $D = 0$ has two roots for a given k_T ,

$$\omega_{\pm} = -\frac{i\sigma}{\sigma^2 + \sigma_{\chi}^2} k_T^2 \pm \frac{\sigma_{\chi}}{\sigma^2 + \sigma_{\chi}^2} k_T \sqrt{k_T^2 - (\sigma^2 + \sigma_{\chi}^2)}. \quad (30)$$

If we focus on the region $k_T \gg \sigma, \sigma_{\chi}$, these can be simplified to

$$\omega_{\pm} = \frac{k_T^2}{i\sigma \pm \sigma_{\chi}}, \quad (31)$$

These two roots are all under the real axis, which means that the advanced solution is vanishing. So the contour integration over ω in the lower half plane picks up these two poles at ω_{\pm} . We can carry out the integration of Bessel functions

$$\begin{aligned} \int_0^{\infty} dk k^2 \exp[-iak^2] J_1(kb) &= -\frac{b}{4a^2} \exp\left[i\frac{b^2}{4a}\right], \\ \int_0^{\infty} dk k \exp[-iak^2] J_0(kb) &= -\frac{i}{2a} \exp\left[i\frac{b^2}{4a}\right]. \end{aligned} \quad (32)$$

Finally we obtain the analytical expressions for the magnetic fields

$$\begin{aligned} B_r(t, \mathbf{x}) &= \theta(t-z) Q \frac{x_T}{8\pi(t-z)^2} \exp\left[-\frac{\sigma x_T^2}{4(t-z)}\right] \\ &\quad \times \left\{ \sigma \sin\left[\frac{\sigma_{\chi} x_T^2}{4(t-z)}\right] - \sigma_{\chi} \cos\left[\frac{\sigma_{\chi} x_T^2}{4(t-z)}\right] \right\}, \\ B_{\phi}(t, \mathbf{x}) &= \theta(t-z) Q \frac{x_T}{8\pi(t-z)^2} \exp\left[-\frac{\sigma x_T^2}{4(t-z)}\right] \\ &\quad \times \left\{ \sigma \cos\left[\frac{\sigma_{\chi} x_T^2}{4(t-z)}\right] + \sigma_{\chi} \sin\left[\frac{\sigma_{\chi} x_T^2}{4(t-z)}\right] \right\}, \\ B_z(t, \mathbf{x}) &= \theta(t-z) Q \frac{1}{4\pi(t-z)} \exp\left[-\frac{\sigma x_T^2}{4(t-z)}\right] \\ &\quad \times \left\{ -\sigma \sin\left[\frac{\sigma_{\chi} x_T^2}{4(t-z)}\right] + \sigma_{\chi} \cos\left[\frac{\sigma_{\chi} x_T^2}{4(t-z)}\right] \right\}. \end{aligned} \quad (33)$$

We see that only B_{ϕ} is non-vanishing at $\sigma_{\chi} = 0$. For a point charge moving in the opposite direction, $v \sim -1$, the magnetic fields [up to $\theta(t+z)$] can be obtained from Eq. (33) by a rotation along any radial axis on the transverse plane at $z = 0$. In this case, B_{ϕ} and B_z change their signs but B_r does not.

One can verify that these fields satisfy the Maxwell equations (1). In the same way, we can also derive analytic formula for electric fields in the relativistic limit but the expressions are much more complicated than magnetic fields.

IV. ELECTRIC FIELDS OF A MOVING CHARGE

In this section, we will derive the analytical expression for electric fields in a medium with both Ohm conductivity and chiral magnetic conductivity. Same as in Section III A, we consider that a charged particle moves in the third direction. Following the procedure similar to Section III A, we obtain

$$\begin{aligned} \begin{pmatrix} E_x \\ E_y \\ E_z \end{pmatrix} (\omega, \mathbf{k}) &= 2\pi i Q \omega \frac{\delta(\omega - k_z v)}{L^2 - \sigma_{\chi}^2 k^2} \\ &\quad \times \left[\frac{L + \sigma_{\chi}^2}{\omega + i\sigma} \begin{pmatrix} k_x \\ k_y \\ k_z \end{pmatrix} + i\sigma_{\chi} v \begin{pmatrix} k_y \\ -k_x \\ 0 \end{pmatrix} - vL \begin{pmatrix} 0 \\ 0 \\ 1 \end{pmatrix} \right]. \end{aligned} \quad (34)$$

With Eq. (14) for \mathbf{B} and Eq. (34) for \mathbf{E} we can verify that the Maxwell equations are really satisfied.

When transforming back to coordinate space, we follow the same procedure as in Section III A and get a form for electric fields similar to Eq. (17) for magnetic fields,

$$\mathbf{E}(t, \mathbf{x}) = -\frac{Q}{v} \int \frac{d\omega dk_T}{(2\pi)^2} \frac{\mathbf{E}'(\omega, k_T)}{D(\omega, k_T)}. \quad (35)$$

In the cylindrical coordinate, $\mathbf{E}'(\omega, k_T)$ is given by

$$\begin{aligned} \begin{pmatrix} E'_r \\ E'_\phi \\ E'_z \end{pmatrix}(\omega, k_T) &= ik_T \omega e^{-i\omega(t-z/v)} \left[\frac{L(\omega, k_T) + \sigma_\chi^2}{i\omega - \sigma} \begin{pmatrix} k_T J_1(k_T x_T) \\ 0 \\ -i(\omega/v) J_0(k_T x_T) \end{pmatrix} \right. \\ &\quad \left. + \begin{pmatrix} 0 \\ -\sigma_\chi v k_T J_1(k_T x_T) \\ v L(\omega, k_T) J_0(k_T x_T) \end{pmatrix} \right]. \end{aligned} \quad (36)$$

But the difference from the case of magnetic fields is: besides the four poles in $1/D(\omega, k_T)$, there is an additional pole in the lower half plane from the first term $\sim 1/(\omega + i\sigma)$ as shown in Eq. (34).

From Maxwell equations, we can obtain E_ϕ from B_r instantly ($E_\phi = -vB_r$),

$$E_\phi = \sigma_\chi \frac{Q}{8\pi} \frac{v^2 \gamma^2 x_T}{\Delta^{3/2}} \left[\gamma(vt - z) + A\sqrt{\Delta} \right] e^A. \quad (37)$$

Generally the integration over k_T in $E_{r,z}$ cannot be worked out analytically due to the term $1/(i\omega - \sigma)$ in Eq. (36). However, at relativistic limit $\gamma \gg 1$, this can be done and we can obtain algebraic expression for $E_{r,z}$,

$$\begin{aligned} E_r &= \frac{Q}{4\pi} \left\{ \frac{\gamma x_T}{\Delta^{3/2}} \left(1 + \frac{\sigma v \gamma}{2} \sqrt{\Delta} \right) - \frac{\sigma}{v x_T} e^{-\sigma(t-z/v)} \left[1 + \frac{\gamma(vt - z)}{\sqrt{\Delta}} \right] \right\} e^A, \\ E_z &= \frac{Q}{4\pi} \left\{ -e^A \frac{1}{\Delta^{3/2}} \left[\gamma(vt - z) + A\sqrt{\Delta} + \frac{\sigma \gamma}{v} \Delta \right] + \frac{\sigma^2}{v^2} e^{-\sigma(t-z/v)} \Gamma(0, -A) \right\}, \end{aligned} \quad (38)$$

where $\Gamma(0, -A)$ is the incomplete gamma function defined as $\Gamma(a, z) = \int_z^\infty dt t^{a-1} \exp(-t)$. We have checked in numerical calculations that the result of Eqs. (37,38) is a good approximation to the exact result for the scale of heavy ion collisions. We have also checked that electric and magnetic fields in Eqs. (37,38) and Eqs. (27,28) satisfy the Maxwell equations (1) in a good accuracy for the scale of heavy ion collisions.

In the leading order in σ_χ , we see in Eqs. (37,38) that E_ϕ is proportional to σ_χ while $E_{r,z}$ are independent of σ_χ . The higher order contributions to E_ϕ , E_r and E_z are all of $O(\sigma_\chi^2)$.

V. NUMERICAL RESULTS FOR ELECTROMAGNETIC FIELDS IN HEAVY-ION COLLISIONS

In this section we will give numerical results for \mathbf{B} and \mathbf{E} from Eqs. (17,35). The source terms are given by the configuration that two nuclei collide with an impact parameter, which is a convolution of the point charge/current density in the form of Eq. (12) with the charge distribution of nuclei.

Fig. (1) shows \mathbf{B} and \mathbf{E} as functions of time at $\mathbf{x} = (0, 0, 0)$ fm produced by a point charge (proton) of 100 GeV located at $(6, 0, 0)$ fm and moving along \mathbf{e}_z . We see that the magnitude of B_ϕ is larger than B_r almost all the time and B_z is much smaller than B_r and B_ϕ . The non-vanishing B_r and B_z is due to the chiral magnetic effect or $\sigma_\chi \neq 0$. We also see that the magnitude of E_r is larger than E_ϕ (just opposite to the magnetic field) and E_z . All field components of \mathbf{B} and \mathbf{E} are damped as the time goes on.

We show in Fig. (2) the geometry of two colliding nuclei in peripheral collisions with the impact parameter b . The global magnetic field of this configuration is along $-\mathbf{e}_y$. In the numerical calculation of \mathbf{B} and \mathbf{E} , we choose $b = 4$ fm for Au+Au collisions at $\sqrt{s} = 200$ GeV. We use UrQMD to simulate the space-time and momentum configurations of charged particles in Au+Au collisions in the case of Lienard-Wiechert potential. After the collisions, the spectator nucleons which do not collide fly by freely while participant nucleons are stopped to produce new particles. Participant nucleons will be treated differently in the cases of non-vanishing medium effects with σ and σ_χ : the rapidity distribution of charged particles produced by participant nucleons has to be modified. In our calculations, we adopt the rapidity distribution in Ref. [33].

Figure 1: The electromagnetic fields at $\mathbf{x} = (0, 0, 0)$ fm produced by a point charge (proton) of 100 GeV which are located at $\mathbf{x} = (6, 0, 0)$ fm and moving along \mathbf{e}_z . We choose following values for conductivities $\sigma = 5.8$ MeV and $\sigma_\chi = 1.5$ MeV.

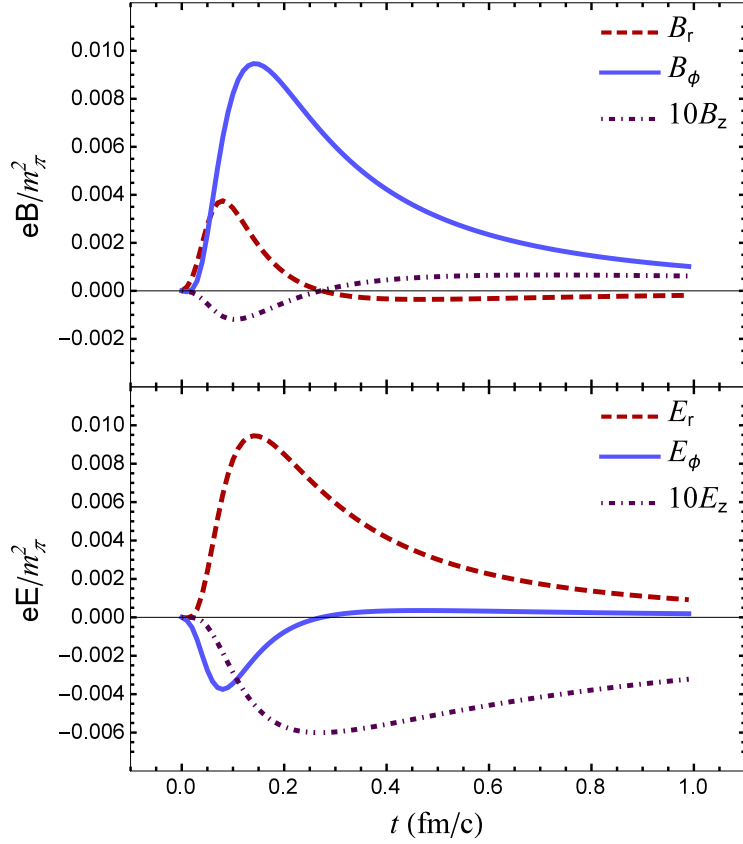
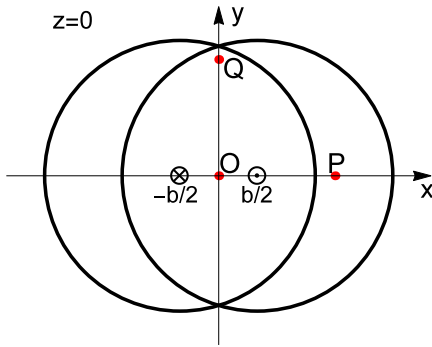


Figure 2: The geometry of two colliding nuclei in the transverse plane at $z = 0$. One nucleus at $(b/2, 0)$ in the transverse plane is moving along \mathbf{e}_z , while another nucleus at $(-b/2, 0)$ is moving along $-\mathbf{e}_z$. The points P and Q in the transverse plane are two typical points at which \mathbf{B} and \mathbf{E} will be calculated.



We show in Figs. (3,4) the time evolution of \mathbf{B} and \mathbf{E} in Au+Au collisions at $\sqrt{s} = 200$ GeV and at two points $(6, 0, 0)$ fm (the point P in Fig. (2)) and $(0, 6, 0)$ fm (the point Q in Fig. (2)). We consider three cases: (a) Lienard-Wiechert potential ($\sigma = \sigma_\chi = 0$, blue solid lines); (b) with only σ ($\sigma \neq 0$ and $\sigma_\chi = 0$, red dashed lines); (c) with both σ and σ_χ ($\sigma \neq 0$ and $\sigma_\chi \neq 0$, magenta dash-dotted lines).

In Fig. (3) we give the time evolution of B_y and E_y at the point $\mathbf{x} = (0, 6, 0)$ fm or the point Q . The x and z components are vanishing, $B_{x,z} \approx 0$ and $E_{x,z} \approx 0$ due to that OQ is along the direction of global orbital angular momentum or global magnetic field. The effect of σ_χ on B_y and E_y is small at late time.

In Fig. (4), we see that B_x , B_z and E_y are mainly controlled by σ_χ , i.e. they are vanishing at

Figure 3: Time evolution of B_y and E_y in Au+Au collisions at $\sqrt{s}=200$ GeV and $\mathbf{x} = (0, 6, 0)$ fm for three cases: (a) Lienard-Wiechert potential ($\sigma = \sigma_\chi = 0$); (b) with σ ($\sigma \neq 0$ and $\sigma_\chi = 0$); (c) with σ and σ_χ ($\sigma \neq 0$ and $\sigma_\chi \neq 0$). The x and z components are vanishing, $B_{x,z} \approx 0$ and $E_{x,z} \approx 0$.

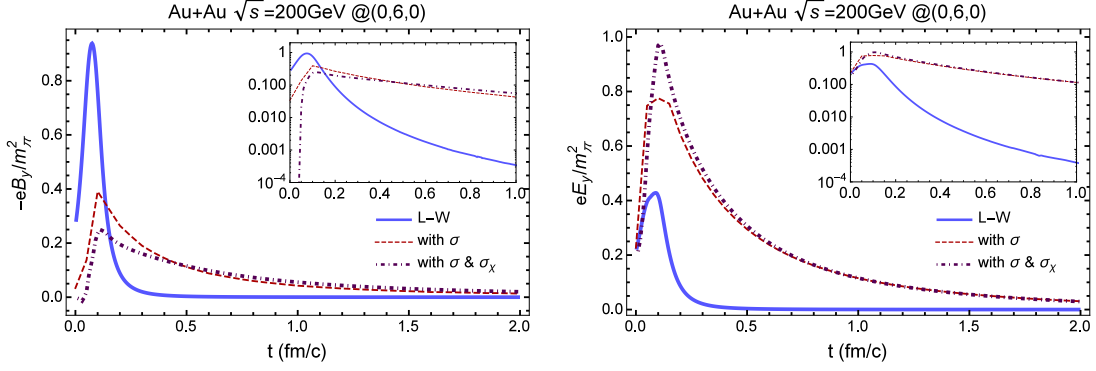


Figure 4: The time evolution of \mathbf{B} and \mathbf{E} in Au+Au collisions at $\sqrt{s}=200$ GeV and $\mathbf{x} = (6, 0, 0)$ fm for three cases: (a) Lienard-Wiechert potential (L-W, $\sigma = \sigma_\chi = 0$); (b) with σ ($\sigma \neq 0$ and $\sigma_\chi = 0$); (c) with σ and σ_χ ($\sigma \neq 0$ and $\sigma_\chi \neq 0$).

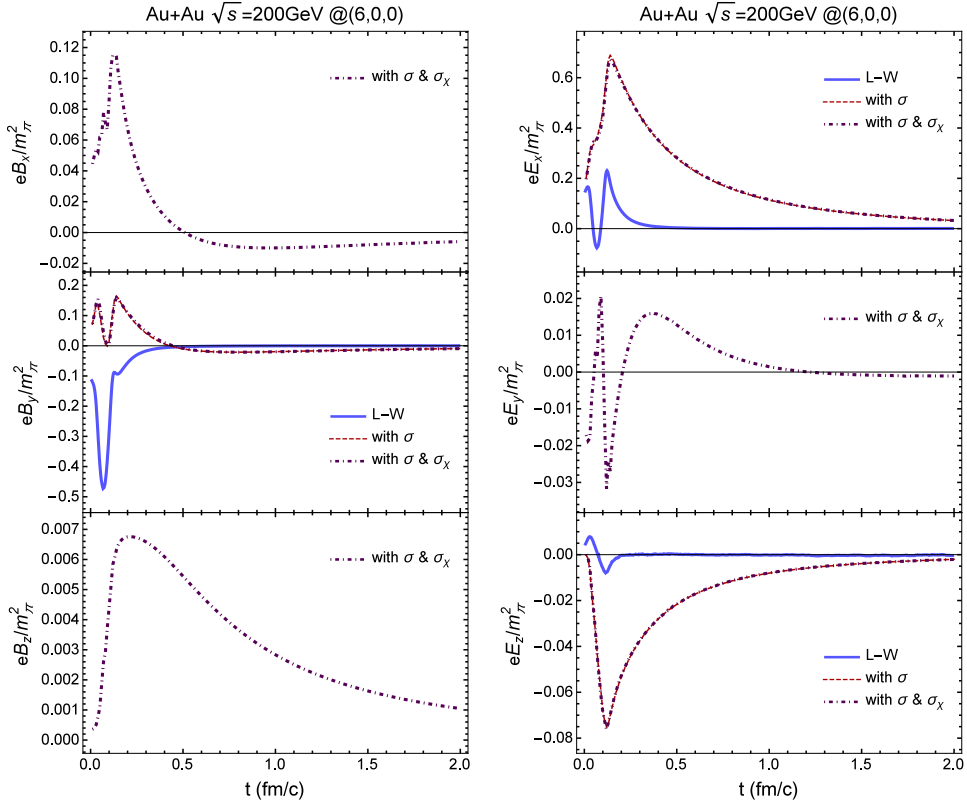


Figure 5: The contour plots for electric (upper panel) and magnetic (lower panel) fields in the transverse plane of $z = 0$ at $t = 2$ fm/c and $\sqrt{s} = 200$ GeV in Au+Au collisions. The two colliding nuclei are shown in two red dashed circles.

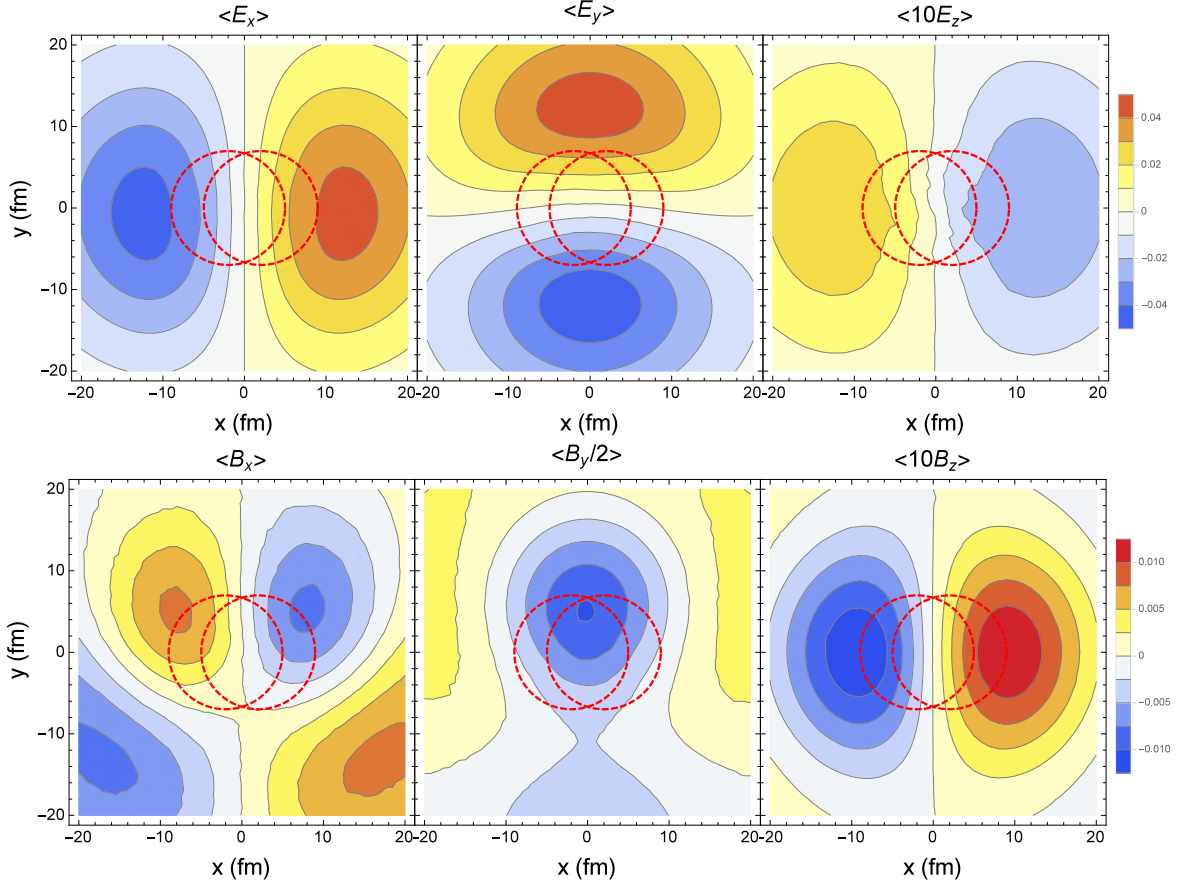


Figure 6: The 2-dimensional vector fields for transverse components \mathbf{B}_T and \mathbf{E}_T in the transverse plane of $z = 0$ at $t = 2$ fm/c and $\sqrt{s} = 200$ GeV in Au+Au collisions.

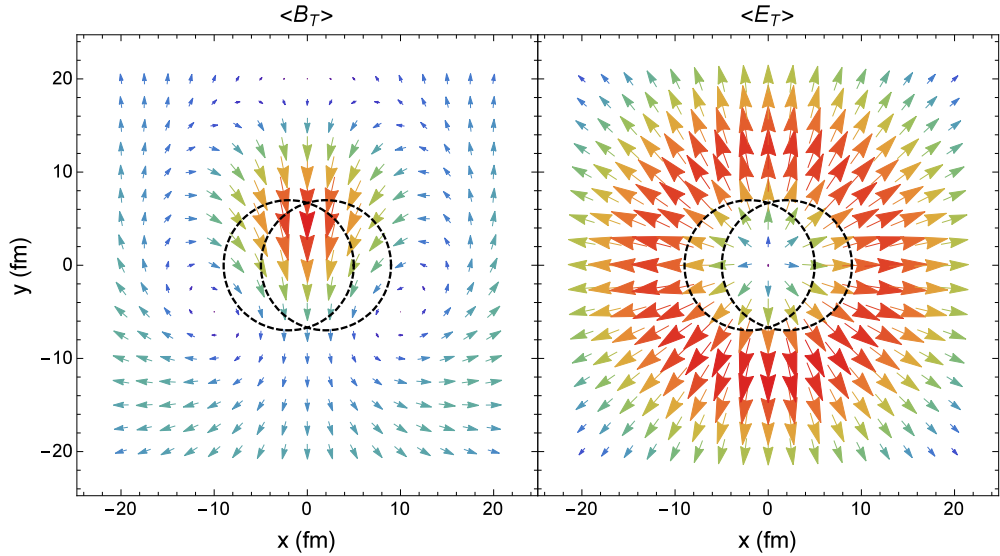
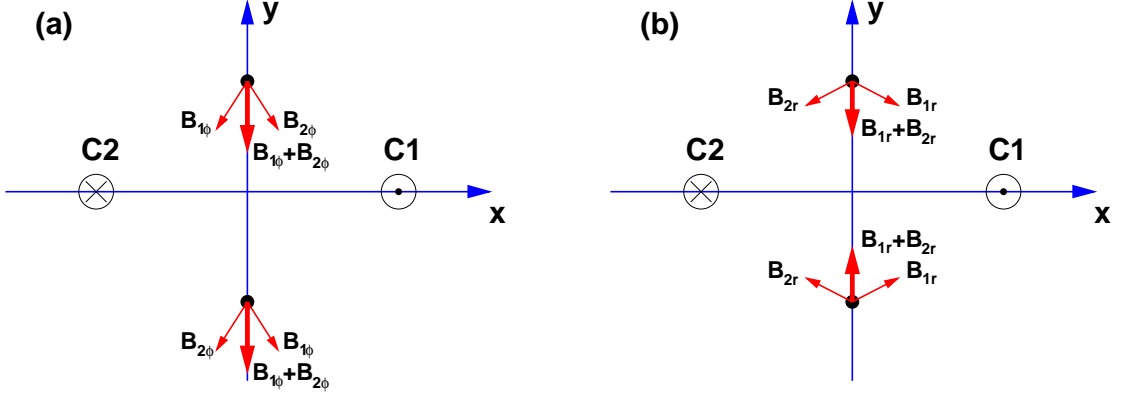


Figure 7: Illustration of the asymmetry of the magnetic fields at non-vanishing σ_χ . Two positive point charges at $(\pm a, 0, 0)$ move in $\pm e_z$ direction. (a) Azimuthal components; (b) Radial components. The azimuthal components are symmetric at symmetric points $(0, \pm b, 0)$, while the radial components have opposite signs.



$\sigma_\chi = 0$. It is interesting to see that B_y has different signs from L-W and from $\sigma \neq 0$ in very short time from the collision moment. The reason is that B_y with L-W is from spectators moving apart rapidly so it is along $-e_y$ and decays quickly in time, but B_y with non-vanishing σ is dominated by the conducting current and lasts longer than the L-W contribution.

The contour plots for electric and magnetic fields in the transverse plane of $z = 0$ are shown in Figs. (5). The time is set to at $t = 2$ fm/c. We see that the magnitudes of x, z components of electric fields $|E_{x,z}(t, x, y, z)|$ are symmetric for flipping the signs of their arguments x and y . The symmetry is partially broken for $|E_y(t, x, y, z)|$ and $|B_{x,y}(t, x, y, z)|$ due to σ_χ : they are symmetric for flipping the sign of x but not for y , while $|B_z(t, x, y, z)|$ preserves the symmetry for flipping the signs of x and y . The field configuration can be more clearly seen in Fig. (6), where the transverse components are shown in two-dimension vectors. We see that \mathbf{E}_T is more symmetric than \mathbf{B}_T in the transverse plane. A magnetic field along $-e_y$ can also be clearly seen near the origin $(0, 0, 0)$. It is obvious that $|B_y(t, x, y, z)| \neq |B_y(t, x, -y, z)|$.

The asymmetry in Figs. (5,6) can be easily understood from non-vanishing B_r resulting from σ_χ . Suppose one positive charge is located at $(a, 0, 0)$ fm and moving along $-e_z$, while the other one is located at $(-a, 0, 0)$ fm and moving along e_z , see Fig. 7. We can compare the magnetic fields at two points, $(0, b, 0)$ fm and $(0, -b, 0)$ fm. For simplicity we assume the relativistic limit and use Eq. (33), where we observe that B_r does not change the sign when flipping the velocity direction. Therefore the direction of radial components of the magnetic fields from two oppositely moving charges at upper point $(0, b, 0)$ fm is opposite to that at lower point $(0, -b, 0)$. But azimuthal components have the same directions and magnitudes at upper and lower point. Thus the total magnetic fields, or the vector sums of radial and azimuthal components, have different magnitude at two symmetric points with respect to the x -axis.

VI. SUMMARY

We have derived analytic expressions for electric and magnetic fields produced by a point charge in a conducting medium with the electric conductivity σ and the chiral magnetic conductivity σ_χ . We used the method of the Green function under the condition $\sigma \gg \sigma_\chi$. We have given in Eqs. (28,37,38) for the first time the algebraic expressions for electric and magnetic fields as functions of space-time without any integrals. Numerical results show that these algebraic results work very well for values of σ_χ which are not very small compared to σ . We have also given the algebraic expressions for magnetic fields at relativistic limit $v = 1$.

The space-time profiles of electromagnetic fields in non-central Au+Au collisions have been calculated based on the above analytic formula as well as the exact numerical method. The UrQMD model was used to simulate the space-time and momentum configurations of charged particles. In collisions, the participant nucleons are treated differently from spectators by introducing a smooth rapidity distribution to account for newly produced charged particles in the central rapidity region. The magnitudes of the axial components of both electric field and magnetic field have the symmetry of flipping the signs of their transverse coordinate arguments x and y . But the magnitudes of transverse

components are only symmetric for flipping the sign of x (in the reaction plane) but not for y . This is the result of the CME.

Combining the space-time evolution of electromagnetic fields with hydrodynamic models or transport models, one can calculate in the future the correlations of charged particles as possible observables of the CME and compare with experimental data.

Acknowledgments. The authors thank L.G. Pang for helpful discussions. Especially QW thanks K. Tuchin for insightful discussions in the Workshop on Chirality, Vorticity and Magnetic Field in Heavy Ion Collisions at UCLA. The authors are supported in part by the Major State Basic Research Development Program (MSBRD) in China under Grant 2015CB856902 and 2014CB845406 respectively and by the National Natural Science Foundation of China (NSFC) under the Grant 11535012.

-
- [1] D. E. Kharzeev, L. D. McLerran, and H. J. Warringa, Nucl. Phys. **A803**, 227 (2008), 0711.0950.
[2] K. Fukushima, D. E. Kharzeev, and H. J. Warringa, Phys.Rev. **D78**, 074033 (2008), 0808.3382.
[3] D. T. Son and P. Surowka, Phys.Rev.Lett. **103**, 191601 (2009), 0906.5044.
[4] D. E. Kharzeev and D. T. Son, Phys.Rev.Lett. **106**, 062301 (2011), 1010.0038.
[5] Y. Burnier, D. E. Kharzeev, J. Liao, and H.-U. Yee, Phys.Rev.Lett. **107**, 052303 (2011), 1103.1307.
[6] Y. Jiang, X.-G. Huang, and J. Liao, Phys. Rev. **D92**, 071501 (2015), 1504.03201.
[7] D. Kharzeev, K. Landsteiner, A. Schmitt, and H.-U. Yee, Lect. Notes Phys. **871**, pp.1 (2013).
[8] D. E. Kharzeev, J. Liao, S. A. Voloshin, and G. Wang, Prog. Part. Nucl. Phys. **88**, 1 (2016), 1511.04050.
[9] D. T. Son and N. Yamamoto, Phys.Rev.Lett. **109**, 181602 (2012), 1203.2697.
[10] M. Stephanov and Y. Yin, Phys.Rev.Lett. **109**, 162001 (2012), 1207.0747.
[11] J.-H. Gao, Z.-T. Liang, S. Pu, Q. Wang, and X.-N. Wang, Phys.Rev.Lett. **109**, 232301 (2012), 1203.0725.
[12] J.-W. Chen, S. Pu, Q. Wang, and X.-N. Wang, Phys.Rev.Lett. **110**, 262301 (2013), 1210.8312.
[13] D. T. Son and N. Yamamoto, Phys.Rev. **D87**, 085016 (2013), 1210.8158.
[14] J.-W. Chen, J.-y. Pang, S. Pu, and Q. Wang, Phys.Rev. **D89**, 094003 (2014), 1312.2032.
[15] C. Manuel and J. M. Torres-Rincon, Phys.Rev. **D89**, 096002 (2013), 1312.1158.
[16] C. Duval and P. Horvathy (2014), 1406.0718.
[17] J.-Y. Chen, D. T. Son, M. A. Stephanov, H.-U. Yee, and Y. Yin, Phys.Rev.Lett. **113**, 182302 (2014), 1404.5963.
[18] D. Satow and H.-U. Yee, Phys.Rev. **D90**, 014027 (2014), 1406.1150.
[19] B. I. Abelev et al. (STAR), Phys. Rev. Lett. **103**, 251601 (2009), 0909.1739.
[20] B. I. Abelev et al. (STAR), Phys. Rev. **C81**, 054908 (2010), 0909.1717.
[21] B. Abelev et al. (ALICE), Phys. Rev. Lett. **110**, 012301 (2013), 1207.0900.
[22] V. Skokov, A. Yu. Illarionov, and V. Toneev, Int. J. Mod. Phys. **A24**, 5925 (2009), 0907.1396.
[23] V. Voronyuk, V. D. Toneev, W. Cassing, E. L. Bratkovskaya, V. P. Konchakovski, and S. A. Voloshin, Phys. Rev. **C83**, 054911 (2011), 1103.4239.
[24] W.-T. Deng and X.-G. Huang, Phys. Rev. **C85**, 044907 (2012), 1201.5108.
[25] J. Błoczynski, X.-G. Huang, X. Zhang, and J. Liao, Phys. Lett. **B718**, 1529 (2013), 1209.6594.
[26] V. Roy and S. Pu, Phys. Rev. **C92**, 064902 (2015), 1508.03761.
[27] H. T. Ding, A. Francis, O. Kaczmarek, F. Karsch, E. Laermann, and W. Soeldner, Phys. Rev. **D83**, 034504 (2011), 1012.4963.
[28] G. Aarts, C. Allton, A. Amato, P. Giudice, S. Hands, and J.-I. Skullerud, JHEP **02**, 186 (2015), 1412.6411.
[29] S. I. Finazzo and J. Noronha, Phys. Rev. **D89**, 106008 (2014), 1311.6675.
[30] K. Tuchin, Phys. Rev. **C88**, 024911 (2013), 1305.5806.
[31] L. McLerran and V. Skokov, Nucl. Phys. **A929**, 184 (2014), 1305.0774.
[32] K. Tuchin, Phys. Rev. **C91**, 064902 (2015), 1411.1363.
[33] U. Gursoy, D. Kharzeev, and K. Rajagopal, Phys. Rev. **C89**, 054905 (2014), 1401.3805.
[34] Z.-W. Lin, C. M. Ko, B.-A. Li, B. Zhang, and S. Pal, Phys. Rev. **C72**, 064901 (2005), nucl-th/0411110.
[35] X.-N. Wang and M. Gyulassy, Phys. Rev. **D44**, 3501 (1991).
[36] S. A. Bass et al., Prog. Part. Nucl. Phys. **41**, 255 (1998), [Prog. Part. Nucl. Phys.41,225(1998)], nucl-th/9803035.
[37] S. Pu, V. Roy, L. Rezzolla, and D. H. Rischke (2016), 1602.04953.